

Cracking of GSO Single Crystal Induced by Thermal Stress

N. Miyazaki¹, T. Tamura², K. Yamamoto¹

Abstract: Quantitative estimation of the failure of a gadolinium orthosilicate (Gd_2SiO_5 , hereafter abbreviated as GSO) single crystal induced by thermal stress was investigated. A GSO cylindrical test specimen was heated in a silicone oil bath, then subjected to large thermal stress by room temperature silicone oil. Cracking occurred during cooling. The transient heat conduction analysis was performed to obtain temperature distribution in the test specimen at the time of cracking, using the surface temperatures measured in the test. Then the thermal stress was calculated using the temperature profile of the test specimen obtained from the heat conduction analysis. It is found from the results of the thermal stress analysis and the observation of the cracking in the test specimens that the cracking induced by thermal stress occurs in a cleavage plane due to the stress component normal to the plane. Three-point bending tests were also performed to examine the relation between the critical stress for the cracking induced by thermal stress and the three-point bending strength obtained from small-sized test specimens. Both sets of failure data obey the Weibull distribution, and the Weibull distribution of the critical stress for the cracking induced by thermal stress can be very well estimated from that of the three-point bending strength by correcting size effect using the Weibull distribution's weakest link model.

keyword: finite element method, thermal stress, cracking, single crystal, crystal anisotropy

1 Introduction

Ce doped GSO single crystal developed by Hitachi Chemical Co. Ltd. is one of the most promising scintillator materials [Takagi and Fukazawa (1983); Ishibashi, Shimizu, Susa, and Kubota (1989)]. Because of its excellent scintillation characteristics, GSO scintillator is expected to be used for medical application such as positron tomograph, as γ -ray detectors for oil well logging application as well as in the field of high energy physics research. GSO bulk single crystals are produced by the Czochralski (CZ) growth technique. Cracking of the crystal sometimes occurs during the CZ growth, especially during cooling down [Ishibashi, Kurata, Kurashige, and Susa (1993)]. The cracking would be caused by thermal stress

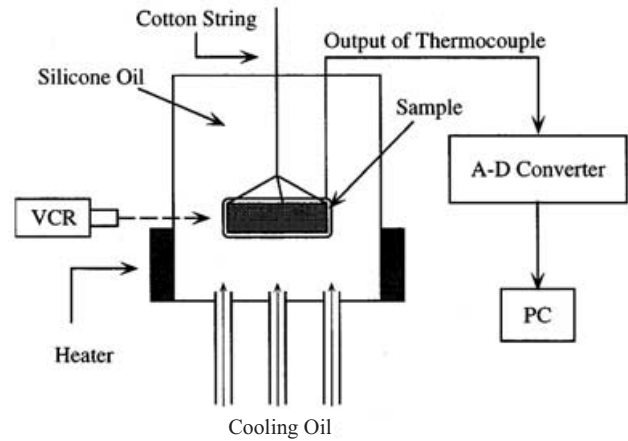


Figure 1 : Equipment for thermal shock tests

during the growth process. It is necessary to perform experiments of cracking induced by thermal stress and their numerical analyses in order to obtain failure stress quantitatively. We have performed such a study on lithium niobate (LN), a trigonal single crystal [Miyazaki, Hattori, and Uchida (1997)].

The objectives of the present study are to obtain what kind of stress dominates the cracking of the GSO single crystal induced by thermal stress and to obtain the failure stress for the cracking. For these purposes, thermal shock tests of the GSO single crystal were carried out, then thermal stress analysis considering crystal anisotropy was performed in order to obtain the critical stress for the cracking induced by thermal stress, using the temperature data obtained from the thermal shock tests. Three-point bending tests were also performed to examine the relation between the critical stress for the cracking induced by thermal stress and the three-point bending strength obtained from small-sized test specimens.

2 Experimental procedure

2.1 Thermal shock tests

Fig. 1 shows the apparatus for the thermal shock tests. Cylindrical test specimens of 50 mm in diameter and 10 mm in thickness shown in Fig. 2 were cut from a GSO bulk single crystal. The surfaces of the test specimens were chemically polished. A test specimen was heated to about 470 K in a bath filled with silicone oil, then thermal shock was applied to it by plunging

¹ Department of Materials Process Engineering, Kyushu University, 6-10-1 Hakozaki, Higashi-ku, Fukuoka, 812-8581 Japan.

² Toyo Information Systems Co. Ltd., 1-13-33, Esaka-cho, Suita, Osaka, 564-0063 Japan.

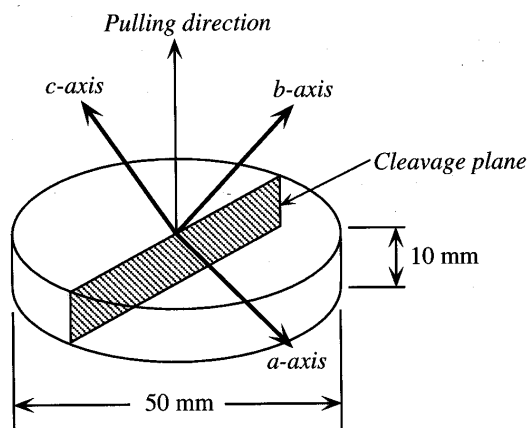


Figure 2 : Test specimen for thermal shock test

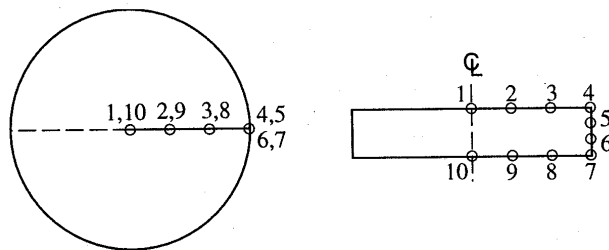


Figure 3 : Locations of temperature measurement

room temperature silicone oil into heated oil bath; cracking occurred during cooling due to thermal stress. The surface temperatures were measured using thermocouples attached on the specimen surfaces and all the measured temperatures were recorded in a personal computer (PC) via an analog-to-digital converter. Fig. 3 shows locations of temperature measurement. The time when the cracking occurred was identified by a video cassette recorder (VCR).

2.2 Three-point bending tests

Three-point bending tests were performed at a temperature of 470 K and at the displacement rate of 0.2 mm/min. The test specimen was 50 mm in length and a square with the sides of 4.5 mm in the cross section. All the surfaces of the test specimens were chemically polished. A GSO is a monoclinic class 2/m single crystal, and the crystallographic *a*-axis is 17.5° inclined from the *b*-*c* plane, as shown in Fig. 4. A right-handed Cartesian coordinate system X_1 - X_2 - X_3 is taken in such a way that the X_2 - and X_3 -axes coincide with the crystallographic *b*-axis [010] and *c*-axis [001], respectively, as shown in Fig. 4. The GSO single crystal has the (100) cleavage plane and the [001] slip direction in the cleavage plane. The three-point bending tests were performed for six cases which have different combinations of the longitudinal direction and the loading

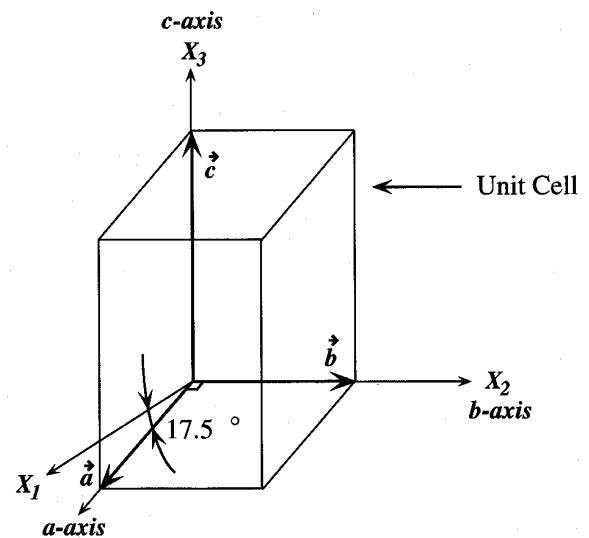


Figure 4 : Crystallographic coordinate system

Table 1 : Test conditions for three-point bending tests

Case	Longitudinal direction	Loading direction
1	X_1	X_2
2	X_1	X_3
3	X_2	X_1
4	X_2	X_3
5	X_3	X_1
6	X_3	X_2

direction, as shown in Tab. 1 and Fig. 5.

3 Analytical procedure

A flowchart for evaluation of thermal shock test results is shown in Fig. 6. Transient heat conduction analysis was performed to obtain the temperature distribution in a GSO test specimen using the surface temperatures measured in the thermal shock test. Thermal stress analysis was performed on the results of the heat conduction analysis, taking account of the crystal anisotropy. Finally the calculated thermal stress was converted into several stresses for failure evaluation.

3.1 Heat conduction analysis

Finite element transient heat conduction analysis for an axisymmetric body was performed to obtain temperature distribution in the GSO thermal shock test specimen at the time of cracking. The surface temperatures were prescribed as a boundary condition, using the temperature data on the crystal surface measured in the thermal shock test. The density ρ ,

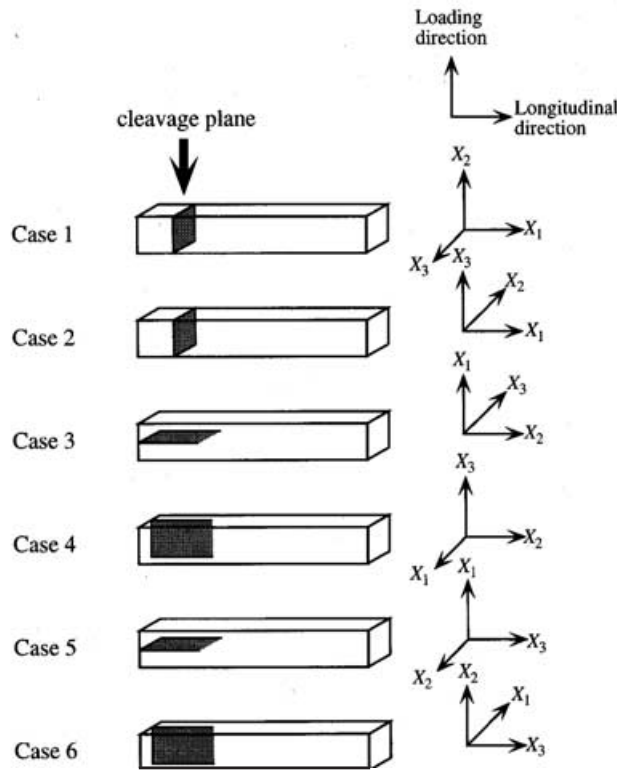


Figure 5 : Test conditions for three-point tests

specific heat C_p and thermal conductivity λ of the GSO single crystal are required for the heat conduction analysis. The following were used in the present analysis:

$$\rho = 6.71 \text{ g/cm}^3, C_p = 350 \text{ J/(kg} \cdot \text{K)}, \lambda = 2.98 \text{ W/(m} \cdot \text{K)}$$

The values of C_p and λ were measured by Hitachi Chemical Co. Ltd. with the laser flash method.

3.2 Thermal stress analysis

Thermal stress analysis was performed using a computer code developed to deal with a monoclinic class $2/m$ single crystal [Miyazaki, Tamura, Kurashige, Ishibashi, and Susa (1997)]. It considers anisotropy in the elastic constants C_{ij} and thermal expansion coefficients α_i , so the code uses the three-dimensional finite element method.

The stress-strain relations of single crystal are given as

$$\sigma_{ij} = C_{ijkl}\epsilon_{kl} \quad (1)$$

where σ_{ij} and ϵ_{ij} are the stress tensors and strain tensors respectively, and C_{ijkl} denote the elastic constant tensors. The matrix components of stress σ_i and strain ϵ_i are related to their correspondent tensor components σ_{ij} and ϵ_{ij} as follows [Nye

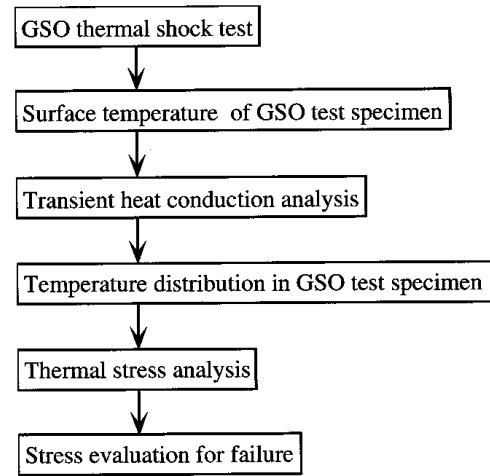


Figure 6 : Flowchart for evaluation of thermal shock test results

(1957)]:

$$\begin{bmatrix} \sigma_{11} & \sigma_{12} & \sigma_{13} \\ \sigma_{21} & \sigma_{22} & \sigma_{23} \\ \sigma_{31} & \sigma_{32} & \sigma_{33} \end{bmatrix} \rightarrow \begin{bmatrix} \sigma_1 & \sigma_6 & \sigma_5 \\ \sigma_6 & \sigma_2 & \sigma_4 \\ \sigma_5 & \sigma_4 & \sigma_3 \end{bmatrix}$$

$$\begin{bmatrix} \epsilon_{11} & \epsilon_{12} & \epsilon_{13} \\ \epsilon_{21} & \epsilon_{22} & \epsilon_{23} \\ \epsilon_{31} & \epsilon_{32} & \epsilon_{33} \end{bmatrix} \rightarrow \begin{bmatrix} \epsilon_1 & \epsilon_6/2 & \epsilon_5/2 \\ \epsilon_6/2 & \epsilon_2 & \epsilon_4/2 \\ \epsilon_5/2 & \epsilon_4/2 & \epsilon_3 \end{bmatrix} \quad (2)$$

Then the stress-strain relations are given by matrix notation as follows:

$$\sigma_i = C_{ij}\epsilon_j \quad (3)$$

For a monoclinic class $2/m$ single crystal such as GSO, the elastic constant matrix is written as follows [Nye (1957)] for the Cartesian coordinate system X_1 - X_2 - X_3 shown in Fig.2:

$$[C_{ij}] = \begin{bmatrix} C_{11} & C_{12} & C_{13} & 0 & C_{15} & 0 \\ & C_{22} & C_{23} & 0 & C_{25} & 0 \\ & & C_{33} & 0 & C_{35} & 0 \\ & & & C_{44} & 0 & C_{46} \\ \text{sym.} & & & & C_{55} & 0 \\ & & & & & C_{66} \end{bmatrix} \quad (4)$$

Let us consider a right-handed Cartesian coordinate system X'_1 - X'_2 - X'_3 shown in Fig. 7, where the X'_3 -axis coincides with the symmetric axis of the test specimen, and the X'_1 -axis is in the X_1 - X_2 plane and normal to the X'_3 -axis. By the standard tensor transformation, the elastic constant tensors C'_{ijkl} associated with the X'_1 - X'_2 - X'_3 system are related to C_{ijkl} of the X_1 - X_2 - X_3 system as follows:

$$C'_{ijkl} = a_{im}a_{jn}a_{ko}a_{lp}C_{mnop} \quad (5)$$

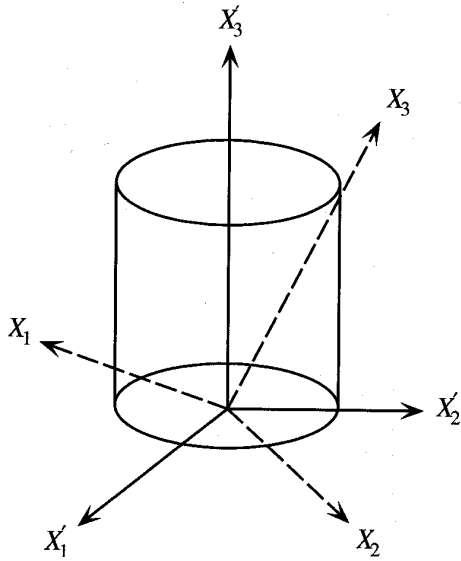


Figure 7 : Coordinate system for thermal stress analysis

For a monoclinic class $2/m$ single crystal, the thermal strain vector $\{\epsilon^T\}$ is given in the X_1 - X_2 - X_3 system as follows [Nye (1957)]

$$\{\epsilon^T\} = \begin{pmatrix} \epsilon_1^T \\ \epsilon_2^T \\ \epsilon_3^T \\ \epsilon_4^T \\ \epsilon_5^T \\ \epsilon_6^T \end{pmatrix} = \begin{pmatrix} \int \alpha_{11} dT \\ \int \alpha_{22} dT \\ \int \alpha_{33} dT \\ \int \alpha_{23} dT \\ \int \alpha_{31} dT \\ \int \alpha_{12} dT \end{pmatrix} = \begin{pmatrix} \int \alpha_1 dT \\ \int \alpha_2 dT \\ \int \alpha_3 dT \\ 0 \\ \int \alpha_5 dT \\ 0 \end{pmatrix} \quad (6)$$

where σ_{ij} and α_i are the thermal expansion coefficient tensors and the components of the thermal expansion vector, respectively. Using the standard tensor transformation, we obtain the thermal expansion coefficient tensors α'_{ij} in the X'_1 - X'_2 - X'_3 system as follows:

$$\alpha'_{ij} = a_{ik} a_{jl} \alpha_{kl} \quad (7)$$

The finite element computer code used in the analysis has the elastic constant matrix and thermal expansion coefficient vector obtained from tensor transformation technique mentioned above. This makes it possible to perform thermal stress analysis of a monoclinic class $2/m$ single crystal in the Cartesian coordinate system X'_1 - X'_2 - X'_3 which is different from the crystallographic coordinate system X_1 - X_2 - X_3 , as shown in Fig. 7. The details of C'_{ijkl} and α'_{ij} are given in Miyazaki, Tamura, Kurashige, Ishibashi, and Susa (1997).

The finite element model for the three-dimensional thermal stress analysis of a GSO test specimen are shown in Fig. 8, where one quarter region is cut in order to show the internal part clearly. The elastic constants and thermal expansion coefficient of the GSO single crystal were respectively measured

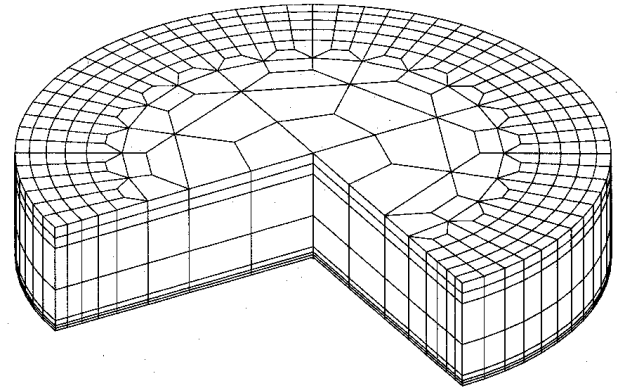


Figure 8 : FEM mesh for three-dimensional thermal stress analysis

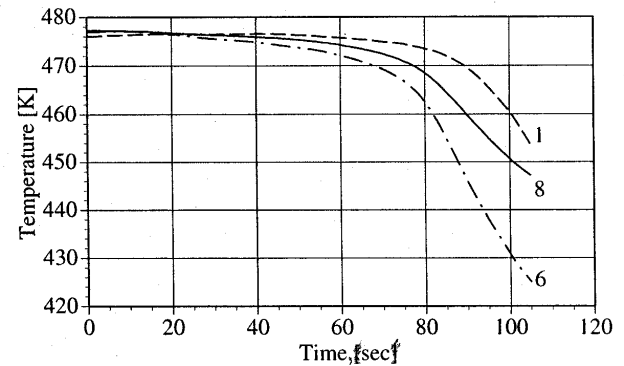


Figure 9 : Time variations of surface temperatures measured by thermocouples

using ultrasonic pulse method [Kurashige, Kurata, Ishibashi, and Susa (1997)] and dilatometer [Utsu and Akiyama (1991)]. They are summarized in Tab. 2, in which the thermal expansion coefficient α_5 is not identified probably because it is small compared with others.

3.3 Stress evaluation for cracking

Thermal stress at the time of cracking obtained from the analysis was converted into the following stresses to discuss the cracking induced by thermal stress : (a) Mises equivalent stress $\sqrt{3J_2}$, (b) the maximum principal stress σ_1 , (c) the normal stress σ_n acting on the (100) cleavage plane, and (d) the maximum shear stress σ_s acting on the (100) cleavage plane.

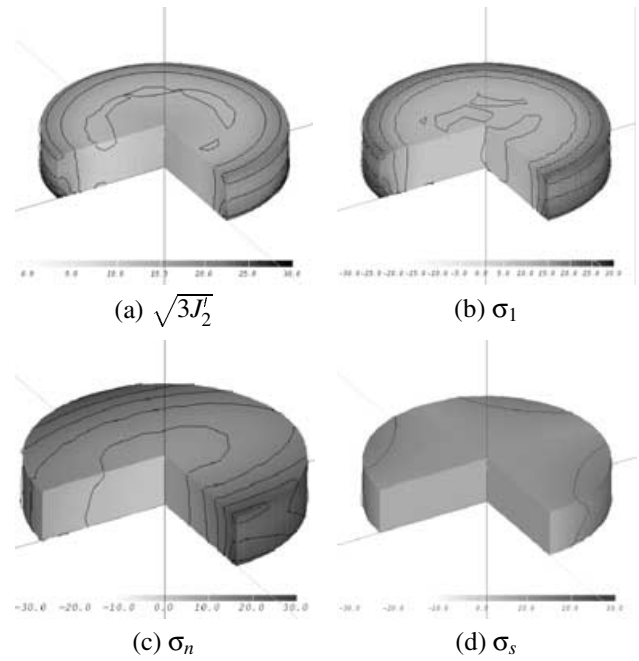
4 Results and discussion

4.1 Thermal shock tests

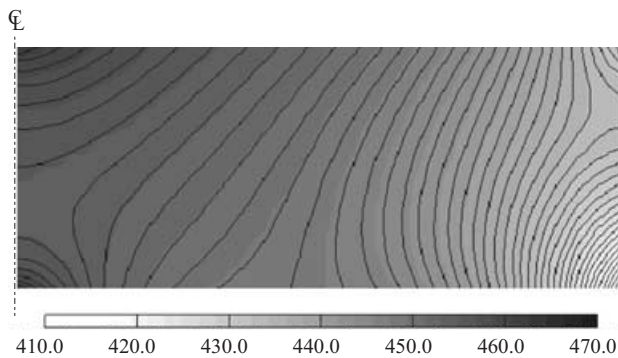
Seven runs of the thermal shock tests were performed. Fig. 9 shows an example of time variations of surface temperatures

Table 2 : Elastic constants and thermal expansion coefficients of GSO single crystal

Const.	Value	Unit
C_{11}	2.23×10^5	[MPa]
C_{12}	1.08×10^5	[MPa]
C_{13}	0.985×10^5	[MPa]
C_{15}	0.084×10^5	[MPa]
C_{22}	1.50×10^5	[MPa]
C_{23}	1.02×10^5	[MPa]
C_{25}	0.333×10^5	[MPa]
C_{33}	2.51×10^5	[MPa]
C_{35}	-0.06×10^5	[MPa]
C_{44}	0.788×10^5	[MPa]
C_{46}	-0.066×10^5	[MPa]
C_{55}	0.688×10^5	[MPa]
C_{66}	0.827×10^5	[MPa]
α_1	4.8×10^{-6}	[K ⁻¹]
α_2	14.0×10^{-6}	[K ⁻¹]
α_3	6.4×10^{-6}	[K ⁻¹]

**Figure 11** : Distributions of stresses obtained from thermal stress analysis (Unit: MPa, $\Delta\sigma = 5$ MPa)

measured by thermocouples which are attached to the locations 1, 6 and 8 shown in Fig. 3. The origin of time is defined at the time when room temperature silicone oil begins to flow into hot silicone oil. In this case, cracking of a test specimen occurs at the time of 90.8 seconds. Using these measured temperatures, transient heat conduction analysis was performed to obtain the temperature distribution at the time of cracking. An example of the calculated result is shown in Fig. 10. Fig. 11 shows the distributions of stresses at the time of cracking obtained from thermal stress analysis. As shown in Fig. 10 and 11, a large temperature gradient was caused near the side wall of the test specimen due to the cooling by room temperature silicone oil and a large thermal stress is therefore induced at the side wall.

**Figure 10** : Temperature distribution obtained from heat conduction analysis (Unit: K, $\Delta T = 1$ K)**Figure 12** : Cracking observed in thermal shock test

The maximum values of various stresses at the time of cracking are summarized in Tab. 3. The cracking shown in Fig. 12 was observed in all the test specimens used in the thermal shock tests. A crack runs straight from the side surface, passing through the center of the specimen. The crack surface is confirmed to be the (100) cleavage plane by X-ray diffraction. Among the four stresses shown in Fig. 11 and Tab. 3, the stress σ_n acting on the cleavage plane can be used to explain the cracking phenomenon. It is found from Fig. 11(c) that σ_n has the maximum at the side surface of the test specimen where the (100) cleavage plane intersects. Therefore, the crack runs along the (100) cleavage plane. It is concluded that among the four stresses evaluated for the cracking, the maximum value of σ_n dominates the cracking induced by thermal stress.

Table 3 : Maximum values of stresses at the time of cracking

sample no.	$\sqrt{3J_2}'$	σ_1	σ_n	σ_s
No-1	16.90	32.22	15.84	8.360
No-2	33.38	70.56	34.61	13.68
No-3	19.01	41.09	20.66	8.105
No-4	30.96	67.41	34.21	9.086
No-5	20.69	44.29	22.35	8.897
No-6	26.03	56.23	29.13	8.297
No-7	33.58	64.55	32.33	16.54
Ave.	25.79	53.76	27.02	10.42

Table 4 : Average value of three-point bending strength

Case	1	2	3	4	5	6
Average σ_b [MPa]	102.5	44.34	151.2	157.3	-	618.2

4.2 Three-point bending tests

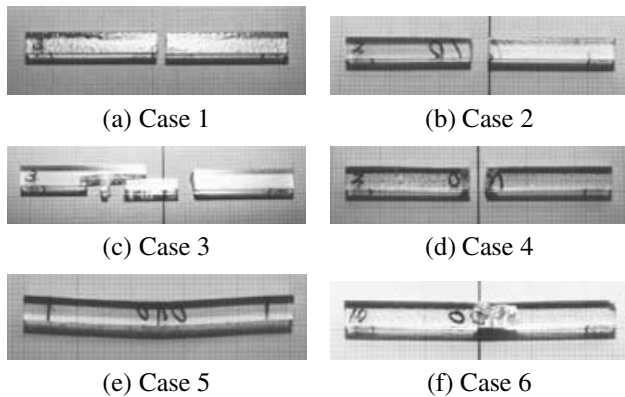


Figure 13 : Failure observed in three-point bending tests

Fig. 13 shows failure modes observed in the three-point bending tests for the six cases of test condition as mentioned in 2.1. In Cases 1, 3, 4 and 6, brittle failure occurred, and rough fracture surfaces are observed. In particular secondary fracture in the cleavage plane along the longitudinal direction is observed in Case 3. In Case 2, slip occurred at first, since the loading direction is parallel to the slip direction. Soon afterwards, failure occurred due to tensile stress, which was caused by the bending moment, normal to the cleavage plane. Very smooth fracture surface is observed in this case, which indicates that cleavage fracture occurred. In Case 5, the direction of longitudinal shear stress is parallel to the slip direction, so slips occurred repeatedly along the longitudinal direction which causes a very

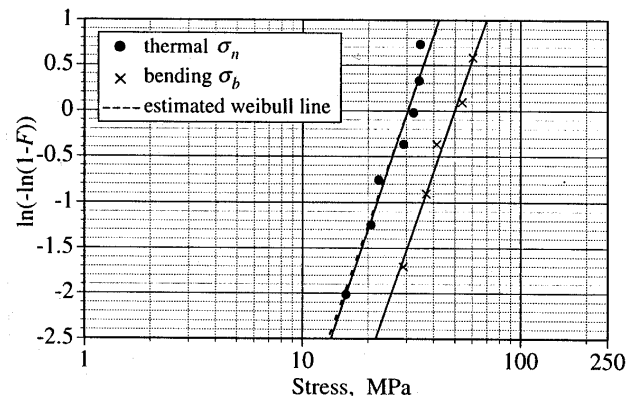


Figure 14 : Weibull plots for failure stress

large deformation without failure, as shown in Fig. 13(e). The average value of three-point bending strength for each case is given in Tab. 4. Since Case 2 has the lowest three-point bending strength and complete cleavage failure are observed both in Case 2 and in the test specimens used in the thermal shock tests, the three-point bending strength for Case 2 should be used to be compared with the critical stress for the cracking induced by thermal stress.

4.3 Relation between thermal shock tests and three-point bending strength

Generally speaking, failure strength of a brittle material is dominated by small defects in the material, and its failure strength deviates greatly due to the deviation of the defect sizes. The deviation of the maximum value of σ_n at the time of cracking obtained from the thermal shock tests shown in Tab. 4 may be due to this reason, so it is appropriate to deal with the failure data statistically. Weibull plots of the failure data obtained from the thermal shock tests and the three-point bending tests are shown in Fig. 14 where the cumulative failure probability F is related to the stress σ_n for the thermal shock tests and the stress σ_b for the three-point bending tests. Both sets of the failure data show good linearity and obey the Weibull distribution. According to the Weibull distribution's weakest link model, the strength of a brittle material is dominated by the maximum size of defect subjected to tensile stress, and the probability of large-sized defects being subjected to tensile stress increases as the specimen size increases. Consequently, a large specimen has lower failure stress. This is why the failure data from the thermal shock tests scatter at lower stress than those from the three-point bending tests. Furthermore, the slopes of both lines are almost the same, which indicates that the Weibull distribution of the thermal shock tests can be estimated from that of the three-point bending tests by correcting size effect using the Weibull distribution's weakest link model. The broken line in Fig. 14 is the Weibull distribution estimated from the three-point bending data. The estimated Weibull dis-

tribution agrees very well with that of the thermal shock tests.

5 Concluding remarks

It is found from the results of thermal stress analysis and the observation of the cracking in GSO test specimens that the cracking induced by thermal stress occurs in the (100) cleavage plane due to the stress component normal to the plane. The failure data obtained from the thermal shock tests and those of the three-point bending tests obey the Weibull distribution, and the Weibull distribution of the thermal stress cracking can be very well estimated from that of the three-point bending strength by correcting size effect using the Weibull distribution's weakest link model.

Acknowledgement: The authors would like to express their gratitude to Hitachi Chemical Co. Ltd. for supplying GSO test specimens. This study was financially supported by a Grant-in-Aid for Scientific Research from the Ministry of Education and Culture.

References

- Ishibashi, H.; Kurata, Y.; Kurashige, K.; Susa, K.** (1993): Crystal growth and scintillation properties of GSO crystal. In *Proceedings of International Workshop on Heavy Scintillators for Scientific and Industrial Applications; CRYSTAL 2000*, pp. 389–393.
- Ishibashi, H.; Shimizu, K.; Susa, K.; Kubota, S.** (1989): Cerium doped GSO scintillators and its application to positron sensitive detectors. *IEEE Transactions on Nuclear Science*, vol. 36, pp. 170–172.
- Kurashige, K.; Kurata, Y.; Ishibashi, H.; Susa, K.** (1997): Mechanical properties of a Gd_2SiO_5 single crystal. *Japanese Journal of Applied Physics*, vol. 36, pp. 2242–2246.
- Miyazaki, N.; Hattori, A.; Uchida, H.** (1997): Thermal shock cracking of lithium niobate single crystal. *Journal of Material Science: Materials in Electronics*, vol. 8, pp. 133–138.
- Miyazaki, N.; Tamura, T.; Kurashige, K.; Ishibashi, H.; Susa, K.** (1997): Thermal stress analysis of GSO bulk single crystal. *Journal of Crystal Growth*, vol. 182, pp. 73–80.
- Nye, J. F.** (1957): *Physical Properties of Crystals*. Clarendon Press.
- Takagi, K.; Fukazawa, T.** (1983): Cerium-activated Gd_2SiO_5 single crystal scintillator. *Applied Physics Letters*, vol. 42, pp. 43–45.
- Utsu, T.; Akiyama, S.** (1991): Growth and application of Gd_2SiO_5 : Ce scintillators. *Journal of Crystal Growth*, vol. 109, pp. 385–391.

